Non-RRKM Dynamics in the CH_3O_2 + NO Reaction System

Philip J. Stimac[†] and John R. Barker*

Department of Atmospheric, Oceanic, and Space Sciences, University of Michigan, Ann Arbor, Michigan 48109-2143

Received: October 15, 2007; In Final Form: December 12, 2007

Quasi-classical trajectory (QCT) calculations on a model potential energy surface (PES) show strong deviations from statistical Rice−Ramsperger−Kassel−Marcus (RRKM) rate theory for the decomposition reaction (1) $CH_3OONO^* \rightarrow CH_3O + NO_2$, where the highly excited CH_3OONO^* was formed by (2) $CH_3O_2 + NO \rightarrow CH_3OONO^*$. The model PES accurately describes the vibrational frequencies, structures, and thermochemistry of the *cis*- and *trans*-CH_3OONO isomers; it includes cis−trans isomerization in addition to reactions 1 and 2 but does not include nitrate formation, which is too slow to affect the decay rate of CH_3OONO^*. The QCT results give a strongly time-dependent rate constant for decomposition and damped oscillations in the decomposition rate, not predicted by statistical rate theory. Anharmonicity is shown to play an important role in reducing the rate constant by a factor of 10 smaller than predicted using classical harmonic RRKM theory (microcanonical variational transition state theory). Master equation simulations of organic nitrate yields published previously by two groups assumed that RRKM theory is accurate for reactions 1 and 2 but required surprising parametrizations to fit experimental nitrate yield data. In the present work, it is hypothesized that the non-RRKM rate of reaction (1) and vibrational anharmonicity are at least partly responsible for the surprising parameters.

Introduction

The reaction of peroxyl radicals with nitric oxide is exceptionally important in the chemistry of Earth's troposphere, because the principal result is conversion of relatively unreactive RO_2 radicals (R = H, organic) to highly reactive RO radicals, accompanied by conversion of nitric oxide, which does not directly absorb sunlight at Earth's surface, to NO_2, which directly absorbs sunlight and photodissociates to produce Odd Oxygen ($O_x = O + O_3$). This reaction constitutes the principal chain-propagation step of the atmospheric photochemical cycle that controls ozone. A curious second pathway[1] produces nitrates ($RONO_2$), which are also produced by the reaction $RO + NO_2$. This pathway is essentially negligible for small R groups but is a third or more of the total reaction yield for large R groups at low temperature and high pressure. Nitrates are relatively inert and comprise perhaps the most important sink for RO_x radicals (HO, HO_2, RO, and RO_2) in the polluted troposphere. Because of chain termination, the steady-state atmospheric ozone levels are very sensitive to the reactions that produce nitrates. Large quantities of organic nitrates are produced from biogenic hydrocarbons.[2−5] Secondary organic aerosol formation comes about from semivolatile reaction products, including nitrates produced via this route.[6−9]

A schematic potential energy surface (PES) for the reaction system is shown in Figure 1. Ignoring conformeric isomers, the generic chemical mechanism is given by the following set of reactions:

$$RO_2 + NO \rightarrow ROONO^* \quad (1)$$

$$ROONO^* \rightarrow RO + NO_2 \quad (2)$$

$$ROONO^* \rightarrow RONO_2^* \quad (3)$$

$$RONO_2^* \rightarrow RO + NO_2 \quad (4)$$

$$RONO_2^* + M \rightarrow RONO_2 + M \quad (5)$$

The asterisk (*) denotes vibrationally excited species, M is a collision partner, and collisional deactivation of ROONO* also takes place but is not shown. Production of $RO + NO_2$ is dominant under most conditions, but yields of organic nitrates ($RONO_2$) become significant at higher pressures, at lower temperatures, and for larger organic groups.[10,11] Because of their importance to atmospheric chemistry, these reactions have been studied very intensely.[12−15] Recently, the reaction system has also become a test-bed for understanding the structure, spectroscopy, and reactivity of the ROONO intermediates.[16−37]

The purpose of the present work is to propose a possible solution to a conundrum that arose from theoretical attempts to explain the experimental organic nitrate yields in the RO_2 + NO reactions. Two recent multiwell, multichannel master equation simulations of these systems were successful in fitting experimental data on organic nitrate formation, but both sets of authors pointed out that the fitting parameters are surprising and possibly unphysical.[34,35]

In the master equation simulations carried out by one of us (Barker et al.[34]), the reaction was modeled along the lines shown by reactions 1−5. It was only reported later[25,26] that the cis and trans isomers of ROONO (referring to the OONO conformation) react in somewhat different ways, but this omission did not affect the major conclusions of the study. The simulations were based on three important assumptions: (a) that statistical Rice, Ramsperger, Kassel, and Marcus (RRKM) theory[38−43] is ac-

* To whom correspondence should be addressed. E-mail: jrbarker@umich.edu.

[†] Present address: Department of Chemistry, University of Montana, Missoula, Montana 59812.

10.1021/jp710016n CCC: $40.75
Published on Web 03/05/2008

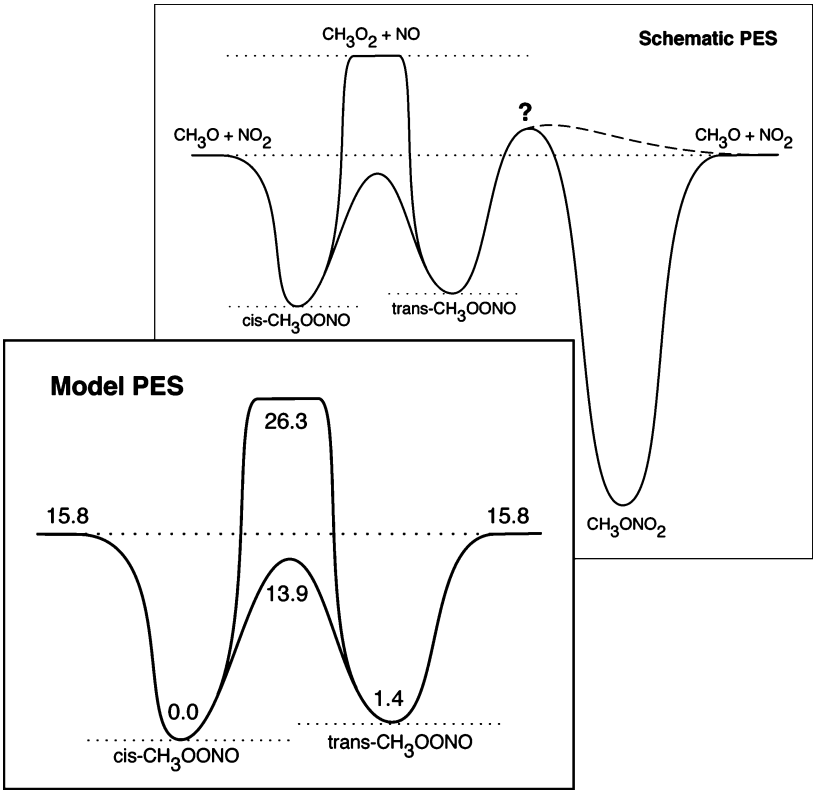

Figure 1. Schematic depiction of the entire potential energy surface as currently understood and of the model PES used in the present calculations. The question mark emphasizes the uncertainties associated with understanding the isomerization reaction from *trans*-CH_3OONO to the $RONO_2$, and the dashed line shows the possible direct connection to the dissociation products. The energies, expressed in units of kcal mol^{-1}, do not include zero-point energy.

curate; (b) that structures and harmonic vibrational frequencies from electronic structure calculations[33] provide accurate sums and densities of states for the RRKM calculations; and (c) that the ratio of dissociation and recombination rate constants is described by the thermodynamic equilibrium constant. Reaction energies were adjusted to fit experimental bond dissociation energies, and for reaction 3 a range of energy barriers and A-factors was investigated, because the electronic structure calculations appeared to be untrustworthy. With these assumptions, the predicted lifetimes of the ROONO* intermediate are so short that they do not experience any collisions at atmospheric pressure. Consequently, pressure effects can only occur if collisional deactivation occurs exclusively in the $RONO_2$ well. Because the lifetime of excited $RONO_2$ is very long, the value of the energy transfer parameter $<\Delta E>_{down}$ needed to fit the data is unusually small. This result led Barker et al. to conclude that either the experimental yield data were in error or that there was some unrecognized deficiency in theoretical understanding. Subsequent experiments by Aschmann et al.[11] confirmed earlier experiments[44−47] from the same laboratory and ruled out experimental artifacts.

Zhang et al.[35] built their master equation simulations in part on some of the results of Lohr et al.[33] and Barker et al.[34] but also included the difference in reactivity of the cis and trans isomers of ROONO.[25,26] They made several major assumptions: (a) statistical RRKM theory is accurate; (b) only *trans*-ROONO can isomerize to form $RONO_2$, and only *cis*-ROONO can dissociate to RO + NO_2; (c) cis−trans isomerization is negligible; (d) the pressure dependence of the $RONO_2$ yields is mostly due to collisional deactivation of *trans*-ROONO* in addition to deactivation of $RONO_2$*; (e) electronic structure calculations for the isomerization reaction are totally unreliable, and a completely empirical model for the transition state is justified; and (f) the isomerization barrier height depends on the identity of R for small groups but is independent of R for larger groups. To satisfy their assumption (d), they adopted very slow rate constants for reaction 2, which controls the lifetime of ROONO*, even though the resulting rate constants do not satisfy the corresponding thermodynamic equilibrium constant and association rate. Even with these assumptions, artificially high pressures were needed to match the experimental yields of $RONO_2$, as they pointed out.

Both master equation simulations were quite detailed and the extensions and many of the additional assumptions made by Zhang et al.[35] are reasonable. Although the philosophical approaches differed, both were state of the art simulations. Although both simulations were able to fit the experimental data on $RONO_2$ yields, it was pointed out in both studies that some unknown fundamental feature was missing from the theoretical models. Both groups subsequently reported master equation simulations on nitric acid formation,[31,32,48] but those studies are not the principal focus of the present paper.

The present work was motivated by the hypothesis that because of slow intramolecular vibrational energy redistribution (IVR), reaction 2 is slower than predicted by RRKM theory, which was assumed to be correct in both master equation simulations. If the lifetime of *cis*-ROONO* is longer than predicted by RRKM theory, then cis−trans isomerization, collisional deactivation, and isomerization to the nitrate will be more competitive with reaction 2. The lengthening of the lifetime would have the same effect as the assumption of slow dissociation made by Zhang et al.[35]

In the following, we present classical trajectory calculations for the CH_3O_2 + NO reaction that clearly show non-RRKM features and quantitative disagreement with RRKM theory. These results support our hypothesis that RRKM theory fails

for this system, but the calculations also show that anharmonicity plays perhaps an even greater role in slowing the unimolecular rate constant. These conclusions must be regarded as tentative, however, because of the approximate nature of the model PES used in the present work.

Methods

To test our hypothesis, we carried out quasi-classical trajectory (QCT) calculations and classical microcanonical variational transition state theory (μVTST) calculations on the model PES described below (see Figure 1). Because RRKM theory is based on μVTST, a significant difference between the QCT and μVTST results on the same PES signals a breakdown of RRKM theory. The thermochemistry of the R = alkyl systems is almost independent of the size of the alkyl group and differs from that of the R = H system.[33] Because CH_3 is the simplest alkyl group, we chose to use R = CH_3 for our calculations.

Model PES. The model PES was constructed by neglecting several reactions. For the purpose of this test, reaction 3 was neglected, because it is much slower than reaction 2 under all conditions and is therefore not important in determining the rate of decay of ROONO*. Furthermore, it is convenient to neglect reaction 3 because its mechanism and transition state are still the subject of considerable debate. Electronic structure calculations on this system are very demanding, but two different mechanisms for reaction 3 have emerged. Dixon et al.[49] and Zhao et al.[25] did not identify a specific transition state for reaction 3, but argued that it occurs via a frustrated dissociation of the RO−ONO bond (on the way toward the RO + NO_2 products). Essentially, the RO−ONO bond elongates but does not completely dissociate. While the bond is elongated, an internal angular motion lines up the O-atom with the N-atom and RO−NO_2 is formed. Chen et al. have observed this type of isomerization in trajectory simulations of the OH + NO_2 reaction on a very complete PES calculated using density functional theory.[37]

A second isomerization pathway has been identified that connects the trans isomer to the nitrate. This pathway has been reported by Ellison et al. for the FO + NO reaction (which is isoelectronic with HO_2 + NO) and by Lesar et al.[50] for the CH_3O_2 + NO reaction (also see ref 51). Both studies have identified specific transition states. Ellison et al.[26] explain their transition state with a curve-crossing model and argue that its energy must be above the RO + NO_2 asymptote. The transition state reported by Lesar et al.[50] for the CH_3O_2 + NO reaction is consistent with that argument. However, Zhang et al.[35] and Zhang and Donahue[32] argue that their model is unable to explain the experimental data unless the transition state energy is considerably below the energy of RO + NO_2. Note that Zhao et al.[25] found an intrinsic energy barrier between the trans isomer and the RO + NO_2 products but did not locate the pathway that leads to the nitrate. Considering these controversies and the difficulties in building a PES that would include reaction 3 and recognizing the fact that reaction 3 is too slow to significantly affect the lifetime of ROONO*, we chose to neglect reaction 3.

The model PES was constructed by using the standard analytical potential energy functions[52] included in a version of *VENUS96*,[53] which has been customized by our group to include additional attenuation functions.[54−56] Initial estimates for parameters were taken from many sources, including electronic structure calculations, measured thermochemistry, and other PESs. Many of the parameters were optimized using a nonlinear least-squares routine. In particular, the equilibrium geometries and harmonic vibrational frequencies for *cis*- and *trans*-CH_3-OONO from Lesar et al.[33] and the thermochemical values from Lohr et al.[33] were used as the basis for the PES. The torsional potential energy barriers (Table 1) for internal rotation about the OO, NO, and OC bonds were computed at the B3LYP/6-311++G** level of theory using the *NWChem* computer program[57] by freezing only the dihedral angle of interest and optimizing all other internal coordinates.

The resulting analytical PES for CH_3OONO consists of five Morse oscillators for bond stretching, five harmonic bends, five dihedral angles (for torsions), and van der Waals nonbonding interactions for atoms separated by ≥2 bonds. The potential energy function is given by eq 6, and the corresponding parameters are listed in Table 1.

$$
\begin{aligned}
V = {} & D_{\mathrm{NO}_a}[1 - \exp^{-\beta_{\mathrm{NO}_a}(r_{\mathrm{NO}_a} - r^0_{\mathrm{NO}_a})}]^2 + \\
& D_{\mathrm{NO}_b}[1 - \exp^{-\beta_{\mathrm{NO}_b}(r^i_{\mathrm{NO}_b} - r^0_{\mathrm{NO}_b})}]^2 + \\
& D_{\mathrm{OO}}[1 - \exp^{-\beta_{\mathrm{OO}}(r^i_{\mathrm{OO}} - r^0_{\mathrm{OO}})}]^2 + \\
& D_{\mathrm{CO}}[1 - \exp^{-\beta_{\mathrm{CO}}(r_{\mathrm{CO}} - r^0_{\mathrm{CO}})}]^2 + \\
& \sum_{i=1}^{3} D_{\mathrm{CH}}[1 - \exp^{-\beta_{\mathrm{CH}}(r^i_{\mathrm{CH}} - r^0_{\mathrm{CH}})}]^2 + \\
& \frac{1}{2} f_{\mathrm{ONO}} S(r_{\mathrm{NO}_a}) S(r^j_{\mathrm{NO}_b})(\theta_{\mathrm{ONO}} - \theta^0_{\mathrm{ONO}})^2 + \\
& \frac{1}{2} f_{\mathrm{NOO}} S(r_{\mathrm{NO}_b}) S(r_{\mathrm{OO}})(\theta_{\mathrm{NOO}} - \theta^0_{\mathrm{NOO}})^2 + \\
& \frac{1}{2} f_{\mathrm{OOC}} S(r_{\mathrm{CO}}) S(r_{\mathrm{OO}})(\theta_{\mathrm{OOC}} - \theta^0_{\mathrm{OOC}})^2 + \\
& \sum_{i=1}^{3} \frac{1}{2} f_{\mathrm{OCH}} S(r_{\mathrm{CO}}) S(r^i_{\mathrm{CH}})(\theta^i_{\mathrm{OCH}} - \theta^0_{\mathrm{OCH}})^2 + \\
& \sum_{i<j}^{3} \frac{1}{2} f_{\mathrm{HCH}} S(r^i_{\mathrm{CH}}) S(r^j_{\mathrm{CH}})(\theta^i_{\mathrm{HCH}} - \theta^0_{\mathrm{HCH}})^2 + \\
& \sum_{n=1}^{3} \frac{k^n_1}{2} S(r_{\mathrm{NO}_a}) S(r_{\mathrm{NO}_b}) S(r_{\mathrm{OO}})[1 + \cos(n\tau_1 - \gamma^n_1)] + \\
& \sum_{n=1}^{3} \frac{k^n_2}{2} S(r_{\mathrm{NO}_b}) S(r_{\mathrm{OO}}) S(r_{\mathrm{CO}})[1 + \cos(n\tau_2 - \gamma^n_2)] + c_1 + \\
& \sum_{i=1}^{3} \sum_{n=1}^{3} \frac{k^n_3}{2} S(r_{\mathrm{OO}}) S(r_{\mathrm{CO}}) S(r_{\mathrm{CH}_i}) \times \\
& [1 + \cos(n\tau_i - \gamma^n_3)] + E_{\mathrm{nonbonded}} \qquad (6a)
\end{aligned}
$$

where the $S(r_{ij})$ terms in eq (6a) are switching functions defined by

$$S(r_{ij}) = \exp[-C(r_{ij} - r^0_{ij})] \qquad (6b)$$

In eq (6b), C is the attenuation constant, and r^0_{ij} is the equilibrium bond distance between atoms i and j.

A schematic energy diagram is shown in Figure 1. Note that both *cis*- and *trans*-CH_3OONO have two chiral stereoisomers (like hydrogen peroxide) and thus there are two transition states of nearly equal energies for the cis−trans isomerization, depending on whether the terminal O-atom rotates out of the OON plane toward or away from the CH_3 group, which is nearly perpendicular to the OON plane.

TABLE 1: Potential Energy Parameters for the Model PES

parameter	value	parameter	value
D_{NO_a}[a]	115.0 kcal mol^{-1}	A_{OO}[h]	370.97 mdyn Å^6/rad^2
D_{NO_b}[b]	26.3 kcal mol^{-1}	A_{CO}	632.78 mdyn Å^6/rad^2
D_{OO}[b]	15.8 kcal mol^{-1}	A_{OH}	36.07 mdyn Å^6/rad^2
D_{CO}[c]	56.9 kcal mol^{-1}	A_{NO}	592.47 mdyn Å^6/rad^2
D_{CH}[d]	102.7 kcal mol^{-1}	A_{CN}	972.33 mdyn Å^6/rad^2
β_{NO_a}[e]	2.906 Å^{-1}	A_{NH}	60.66 mdyn Å^6/rad^2
β_{NO_b}[e]	2.889 Å^{-1}	B_{OO}[h]	−17.65 mdyn Å^{12}/rad^2
β_{OO}	2.289 Å^{-1}	B_{CO}	−19.59 mdyn Å^{12}/rad^2
β_{CO}[e]	2.375 Å^{-1}	B_{OH}	−2.88 mdyn Å^{12}/rad^2
β_{CH}[e]	1.898 Å^{-1}	B_{NO}	−21.16 mdyn Å^{12}/rad^2
f_{ONO}[e]	1.606 mdyn Å/rad^2	B_{CN}	−23.03 mdyn Å^{12}/rad^2
f_{NOO}	1.781 mdyn Å/rad^2	B_{NH}	−3.54 mdyn Å^{12}/rad^2
f_{OOC}	1.143 mdyn Å/rad^2	$r^0_{NO_a}$[i]	1.1593 Å
f_{OCH}	0.847 mdyn Å/rad^2	$r^0_{NO_b}$	1.4718 Å
f_{HCH}	0.497 mdyn Å/rad^2	r^0_{OO}	1.433 Å
k^1_1[f]	0.20 kcal mol^{-1}	r^0_{CO}	1.4308 Å
k^2_1	13.0 kcal mol^{-1}	r^0_{CH}	1.092 Å
k^3_1	1.13 kcal mol^{-1}	θ^0_{ONO}[i]	115.26°
γ^n_1	180.0 degrees (for all n)	θ^0_{NOO}	112.48°
k^1_2	9.86028 kcal mol^{-1}	θ^0_{OOC}	107.77°
k^2_2	5.67642 kcal mol^{-1}	θ^0_{OCH}	109.5°
k^3_2	1.3131 kcal mol^{-1}	θ^0_{HCH}	109.5°
γ^n_2	0.0 degrees (for all n)	τ_1[i]	−0.02°
c_1	−5.14707 kcal mol^{-1}	τ_2	180.0°
k^1_3	0.0 kcal mol^{-1}	τ_3	60.0°
k^2_3	0.0 kcal mol^{-1}	τ_4	−60.0°
k^3_3[g]	0.7146 kcal mol^{-1}	τ_5	109.4°
γ^n_3	0.0 degrees (for all n)	all C	2.0 Å^{-1}

[a] From Benson,[80] who was cited by Preiskorn and Thompson.[81] [b] Based on D_o computed by Lohr et al.[33] [c] From Preiskorn and Thompson.[81] [d] From McKee.[82] [e] The selected β_{ij} and all f_{ijk} values were obtained after initializing a nonlinear least-squares routine with values from Preiskorn and Thompson.[81] [f] This work. The torsional potential energy profiles were fitted using the torsional potential energy functions in eq 1. Barriers to internal rotation: 13.5, 12.0, and 3.25 kcal mol^{-1} for the ONOO, the NOOC, and the HCOO dihedral angles, respectively. [g] k^3_3 is the barrier to internal rotation (3.25 kcal mol^{-1}) divided by 3 (the number of equivalent HCOO dihedral angles). [h] Values from the AMBER[83] force field. [i] Equilibrium values used in the simulations.

The model PES is in reasonable agreement with electronic structure calculations and thermochemistry for the reaction. For example, the equilibrium geometries and vibrational frequencies (Table 2) for *cis*- and *trans*-CH_3OONO are in excellent agreement with the calculated values from Lesar et al.,[33] which were the basis for the PES. The calculated harmonic vibrational frequencies for NO, NO_2, CH_3O, and CH_3O_2 computed on the model PES (Table 3) are in reasonable agreement with previous work (for example, see Barker et al.[34]). The thermochemistry (Figure 1) is in excellent agreement with the results of Lohr et al.[33] and shows that nascent chemically activated ROONO* possesses nearly twice as much energy as needed to break the O−O bond. A minor deficiency is the absence of the small intrinsic energy barrier (i.e., the local maximum on the PES) for *trans*-$CH_3OONO \rightarrow CH_3O + NO_2$.

It is important to note that in the present model PES, all of the attenuation constants (C) in eq 6b and Table 1 were set to $C = 2.0$ Å^{-1}, because QCT calculations using that value produced capture rate constants in fair agreement with typical experimental rate constants for $RO_2 + NO$ reactions.[10,14,15] Thus, the present model PES is reasonable, but a more accurate PES can only be constructed by carrying out many more electronic structure calculations to determine the individual attenuation constants.

QCT Calculations. The bimolecular collision trajectories were initialized with vibrational energy (E^0_{NO}) in the NO

TABLE 2: Vibrational Frequencies (cm^{-1}) of *cis*- and *trans*-CH_3OONO

cis-CH_3OONO		*trans*-CH_3OONO	
B3LYP[a] /6-311++G(d,p)	model PES	B3LYP[a] /6-311++G(d,p)	model PES
63	64	91	81
190	192	187	182
285	286	209	193
320	307	371	303
433	416	410	430
512	533	511	509
781	778	752	645
929	933	971	959
996	981	1011	993
1164	1141	1164	1141
1205	1162	1210	1161
1448	1445	1443	1445
1465	1445	1464	1445
1503	1581	1503	1581
1787	1794	1798	1780
3027	3001	3022	3001
3105	3121	3025	3122
3128	3122	3127	3122

[a] Harmonic frequencies from Lesar et al.,[50] who also give mode assignments.

TABLE 3: Vibrational Frequencies (cm^{-1}) of Reactant/Product Species Computed on the Model PES

NO:	1752
NO_2:	559, 918, 1776
CH_3O:	954, 1131, 1131, 1436, 1436, 1581, 3001, 3121, 3121
CH_3O_2:	214, 379, 549, 972, 1138, 1161, 1445, 1445, 1581, 3001, 3121, 3122

usually set equal to its zero-point energy (2.5 kcal mol^{-1}) and up to 30 kcal mol^{-1} of vibrational energy (E^0_{ROO}) distributed microcanonically[58] in CH_3O_2, which has a zero-point energy of 25.9 kcal mol^{-1} (see Table 3 for the vibrational frequencies of reactants and products on the model PES). We used this method instead of quasi-classical normal mode sampling (another option in *VENUS96*) because we wanted to systematically reduce the initial vibrational energy below the zero-point energy to see if any non-RRKM effects disappear at lower energies. The translational and rotational energies were chosen from Boltzmann distributions at 300 K. The maximum impact parameter was set at 6 Å, where the integral reaction cross section has converged to ≥95% of the asymptotic value. Batches of 10^5 trajectories were run. The initial distance between the two reactants was 10 Å, and the trajectories were terminated after the two products were 10 Å apart.

For the purpose of comparing the trajectory and μVTST results, it is convenient to use the active energy in the nascent complex. The "active" energy is the energy that, according to RRKM theory, can be randomized in the complex. The total excitation energy in a nascent CH_3OONO complex originates from the vibrational and rotational energy of the reactants, the one-dimensional relative translational energy, and the reaction exothermicity. For an ensemble of trajectories for this system, the sum of the average thermal translational and rotational energies is $3RT$. The active energy does not include two rotational degrees of freedom of the complex that are needed to satisfy conservation of angular momentum. These two degrees of freedom contain $\sim RT$ of rotational energy, giving a net contribution of $\sim 2RT$ of active energy from the relative translation and rotations. When this energy is combined with the initial vibrational energy in the reactants and the reaction exothermicity, the active energy is $\sim(2RT + E^0_{NO} + E^0_{ROO} +$

26.3 kcal mol^{-1}) in nascent *cis*-CH_3OONO and 1.4 kcal mol^{-1} lower in *trans*-CH_3OONO. When $E^0_{ROO} = 30$ kcal mol^{-1}, the nascent active energy is ~60.0 kcal mol^{-1} and ~58.6 kcal mol^{-1}, for *cis*- and *trans*-CH_3OONO, respectively, measured from the minimum of the potential in each well. Note that initializing the trajectories with exactly the zero-point energy ($E^0_{ROO} = 25.9$ kcal mol^{-1}) would produce 55.9 kcal mol^{-1} active energy excitation in the *cis* isomer. The figures are labeled with the active energy in the nascent *cis* isomer.

We considered only the lifetimes of CH_3OONO* that formed complexes between NO + CH_3O_2 and that dissociated to NO_2 + CH_3O after ≥3 classical turning points of the CH_3O_2−NO center-of-mass distance. Most calculations were carried out without distinguishing between *cis*- and *trans*-CH_3OONO, but in one batch of trajectories the OONO dihedral angle was calculated, enabling us to make that distinction. The lifetimes of the complexes were recorded as the time during which both the newly formed O−N bond length and the old O−O bond length were ≤2.5 Å. This criterion is arbitrary, but tests showed that the results are not affected significantly as long as this critical distance is greater than ~2 Å.

From the lifetime data, "survival probability" plots were constructed by plotting the fractional number of undissociated complexes as a function of time after their formation. RRKM theory predicts that the population of a monoergic ensemble of complexes should decay exponentially.[59] It is convenient to define an effective first-order rate constant for the decay of population ($N(E,t)$) and survival probability

$$k_{eff}(E,t) = -\frac{\mathrm{d}\ln[P(E,t)]}{\mathrm{d}t} \tag{7}$$

where $P(E,t) = N(E,t)/N(E,0)$ is the survival probability as a function of excitation energy and time, and $k_{eff}(E,t)$ is the effective rate "constant", which may be a function of time. For a pure exponential decay, $k_{eff}(E)$ is independent of time. For the present QCT calculations, the ensemble of nascent complexes is described by a nearly monoergic chemical activation distribution.[38−43] Liu and Barker[60] confirmed that the nascent energy distribution of complexes calculated by *VENUS96* is essentially exactly equal to the one calculated using statistical unimolecular rate theory. Thus, the survival probability curve obtained for a given active energy can be used to obtain $k_{eff}(E,t)$.

Trajectory simulations were also carried out by using microcanonical normal mode sampling[58] of energy in the CH_3OONO* excited complex. The rate constant ($k_{\mu can}(E)$) describing the initial decay of the complexes initialized using the microcanonical energy distribution corresponds to statistical RRKM theory and directly incorporates the effects of anharmonicity.[61] If IVR is rate limiting, the initial microcanonical distribution relaxes to a new steady-state distribution, and the corresponding unimolecular rate constant $k_{ss}(E)$. Given enough time, the intramolecular energy distribution is expected to relax to the steady-state distribution, regardless of how the complexes are initially excited. Thus, one expects $k_{eff}(E,\infty)$ from complexes initially formed by chemical activation to equal $k_{ss}(E)$ from complexes initially formed with a microcanonical energy distribution.

Harmonic μVTST Calculations. According to statistical RRKM rate theory,[38−43] the rate constant $k(E,J)$ is given by

$$k(E,J) = \frac{1}{h}\left[\frac{m^\dagger}{m}\frac{\sigma_{ext}}{\sigma^\dagger_{ext}}\right]\frac{g^\dagger_e}{g_e}\frac{G^\dagger_{vr}[E - V - E^\dagger_r(J)]}{\rho[E - E_r(J)]} \tag{8}$$

where $\rho(x)$ is the rovibrational density of states for the reactant at energy x, $G^\dagger_{vr}(x)$ is the rovibrational sum of states of the transition state, m and $m^\dagger$ are, respectively, the number of optical isomers for the reactant and transition state, σ_{ext} and $\sigma^\dagger_{ext}$ are the external rotational symmetry numbers for the reactant and transition state, and g_e and $g^\dagger_e$ are the electronic degeneracies of the reactant and transition state, respectively. In the present work, we assume that the reactant and transition state have equal numbers of optical isomers, equal symmetry numbers, and equal electronic degeneracies.

To calculate the sum and density of states, vibrational frequencies, moments of inertia, and potential energy along the reaction path are required. The reactant and transition state for reaction 2 were modeled as a collection of s independent classical harmonic oscillators and free rotors to obtain the microcanonical rate constant, $k(E,J)$, which also depends on the quantum number J for total angular momentum. This approach often gives accurate results, when compared to more flexible models.[62−64] To compute $k(E,J)$ using μVTST, we first determine the vibrational frequencies, moments of inertia and potential energy along the reaction path using the canonical variational transition state module included in *VENUS96*.

The rotational energy of the system along the reaction path is approximated by the "almost symmetric top" treatment for which the rotational energy is given by[65,66]

$$E_r(J,K) = \left(\frac{1}{I_a} + \frac{1}{I_b}\right)\frac{[J(J+1) - K^2]h^2}{16\pi^2} + \frac{K^2h^2}{8\pi^2 I_c} \tag{9}$$

where I_a and I_b are the two nearly equal moments of inertia, I_c is the moment of inertia for the K-rotor and J and K are the rotational quantum numbers.

We consider two of the many possible approaches[65,67] for modeling energy exchange between the active K-rotor and the vibrational degrees of freedom. In Method I, we assume that the K-rotor exchanges energy statistically with the vibrational degrees of freedom in both the transition state and in the excited reactant with no restrictions on the amount of energy resident in the K-rotor. According to this method, the rovibrational density of states of the reactant is the convolution of the vibrational density of states and the density of states of the K-rotor and is given by

$$\rho[E - E_r(J)] = \int_0^{E - E_r(J)} \frac{x^{s-1}}{(s-1)!\prod_{i=1}^{s} h\nu_i} \times \{B[E - E_r(J) - x]\}^{-1/2}\,\mathrm{d}x \tag{10}$$

where E is the total energy, $E_r(J)$ is the J-dependent component of the rotational energy, B is the rotational constant of the reactant, the quantity $E - E_r(J)$ is the total active energy in the reactant, and s is the number of harmonic oscillators in the reactant ($s = 18$ for methyl peroxynitrite). Similarly, the rovibrational sum of states of the transition state is given by

$$G^\dagger_{vr}[E - V^\dagger - E^\dagger_r(J)] = \int_0^{E - V^\dagger - E^\dagger_r(J)} \frac{x^{s-1}}{(s-1)!\prod_{i=1}^{s-1} h\nu_i} \times \{B^\dagger[E - V^\dagger - E^\dagger_r(J) - x]\}^{-1/2}\,\mathrm{d}x \tag{11}$$

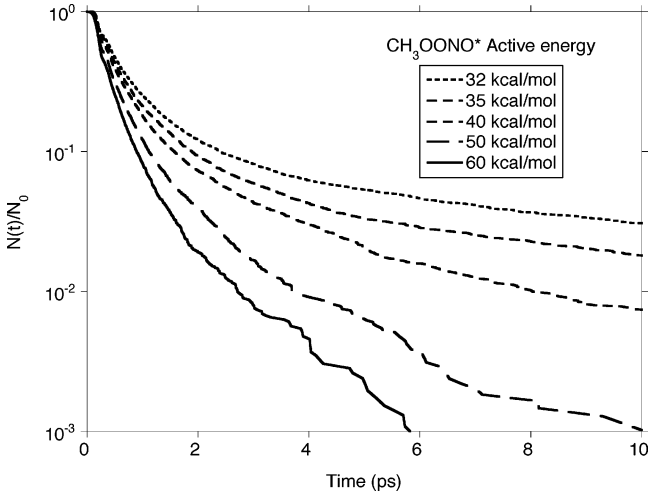

Figure 2. Survival probability curves for various active energies of the nascent CH_3OONO^* formed by the recombination reaction.

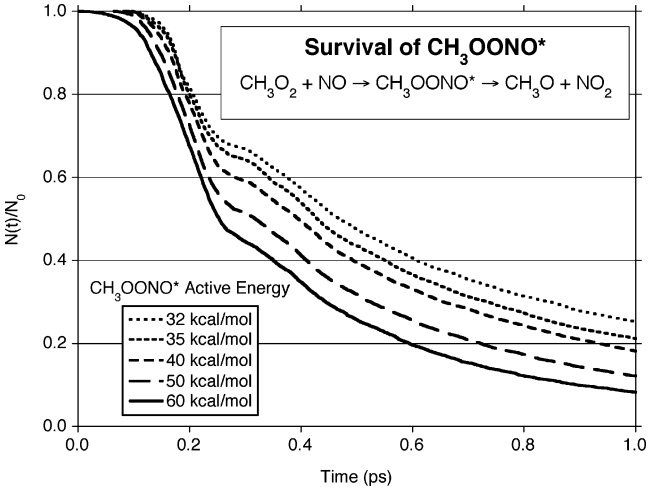

Figure 3. The results from Figure 2 shown on an expanded scale.

where $B^\dagger$ is the rotational constant for the transition state, $E_r^\dagger(J)$ is the J-dependent component of the rotational energy for the transition state, $V^\dagger$ is the classical potential energy at the position of the transition state (the zero of energy is at the bottom of the potential well), $s = 18$, and the quantity $E - V^\dagger - E_r^\dagger(J)$ is the total active energy in the transition state.

To determine $k(E,J)$ variationally for fixed energy E and angular momentum J, we determine the point along the reaction path that gives the minimum rovibrational sum of states according to eq 11, and then compute $k(E,J)$ using eq 8. This protocol for computing $k(E,J)$ is referred to as Method I.

According to Method II for treating the active energy in the K-rotor, the K quantum number is limited to the range $-J \leq K \leq J$, as required for rigid rotors.[65,67] According to this method, the sum of states of the transition state and the density of states of the reactant are given by

$$G_{vr}^\dagger(E,J) = \sum_{K=-J}^{J} G_{vr}^\dagger[E - V^\dagger - E_r^\dagger(J,K)] \qquad (12a)$$

$$\rho(E,J) = \sum_{K=-J}^{J} \rho[E - E_r(J,K)] \qquad (12b)$$

With both methods of treating the active K-rotor, the μVTST rate constant $k(E,J)$ is determined for fixed E and J by finding the minimum $G_{vr}^\dagger(E,J)$, which is given by eq 11 or 12a, and computing $k(E,J)$ using eq 8. With both methods, the average rate constant for the thermal rotational distribution, $\langle k(E,J)\rangle$, is approximated by using $\langle k(E,J)\rangle \approx k(E,\langle J\rangle)$ with $\langle J\rangle = 27$, the average value at 300 K.

Results and Discussion

QCT Calculations. Using the protocol described above, batches of trajectories were carried out with initial vibrational energies in the CH_3O_2 reactant ranging from 0 to 30 kcal mol^{-1}. Most runs included zero-point energy in the nitric oxide, but to reduce the active energy still more, some runs were carried out with no initial vibrational energy in the nitric oxide. The active energies investigated range from 27.5 to 60 kcal mol^{-1}. About 4−7% of the trajectories in each batch of 10^5 resulted in formation of a highly excited CH_3OONO^* complex, very nearly equally distributed between the cis and trans isomers. From the lifetimes of the complexes in each batch, survival probability plots were constructed as described above, and the results are shown on a semilogarithmic scale in Figure 2. The first 1 ps of the survival probabilities is shown on a linear scale in Figure 3.

In Figure 2, all of the survival probabilities decay rapidly at early times and more slowly at later times. In Figure 3, a short delay time is apparent, followed by a decay that resembles a damped oscillation. The short delay time is mostly due to the decision to start the clock when the newly formed O−N bond is 2.5 Å. At 300 K, the average initial relative speed of the RO_2 and NO is ∼3.7 Å ps^{-1}. The short delay time is ∼0.1 ps, which corresponds to a distance of ∼0.4 Å in the absence of intermolecular forces, which are small at these distances. Therefore, starting the clock when the new bond shortens to ∼2.1 Å would eliminate the delay time if all of the collisions took place at the average initial speed. This distance is consistent with our tests, which showed that the results were not affected significantly for distances ≥2 Å. Considering the distribution of initial speeds, the observed brief delay and the initial shape of the survival probability curves is quite reasonable. At slightly longer times, however, the curves are more surprising.

Immediately after the short delay, all of the survival probability curves show a sharp decay, followed by a brief tendency to level off, which is then followed by a more rapid decay that tends toward an exponential at longer times. The initial sharp decay has almost the same slope in all of the plots, showing that the initial rate of decay is rapid and almost independent of the active energy in the system. The initial value of $k_{eff}(E,0)$ calculated using eq 6 to fit the survival probabilities over the time period from ∼0.15 to ∼0.25 ps is shown in Figure 4 for all of the active energies. After several picoseconds have elapsed, the decay of each survival probability curve seems to become exponential. These "final" values of $k_{eff}(E,\infty)$ are strong functions of energy: the highest energy system (60 kcal mol^{-1}) decays more than 100 times faster than the lowest energy system (27.5 kcal mol^{-1}), as shown in Figure 4.

A single batch of trajectories was calculated in which the OONO dihedral angle was evaluated. This enabled us to identify the *cis* and *trans*-CH_3OONO isomers separately. The results showed that the fraction of complexes initially formed was almost equal for the two isomers (52% cis and 48% trans). Furthermore, the cis−trans isomerization reaction was so slow that only 10−15% of the complexes isomerized. This result is consistent with the relatively slow rate constants for isomerization computed in both of the master equation simulations

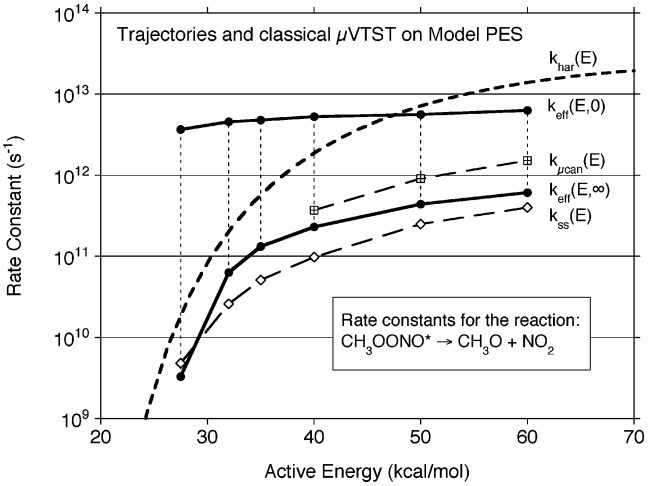

Figure 4. Rate constants calculated from trajectories and from classical harmonic μVTST (according to Method II for the K-rotor and all attenuation constants set to $C = 2$ Å^{-1}). See the text for definitions.

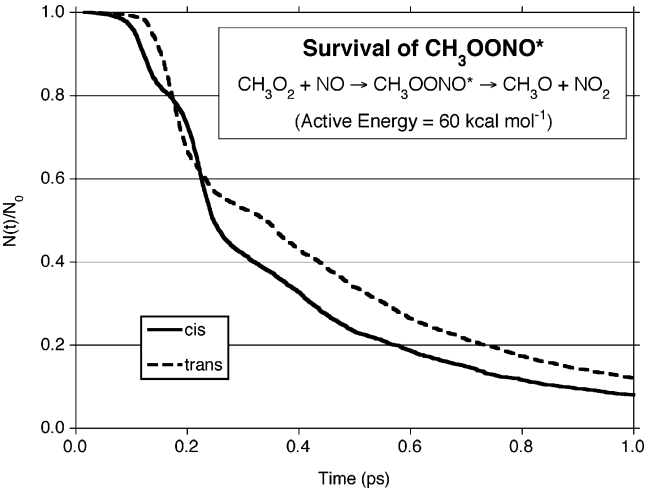

Figure 5. Survival probability curves for the individual chemically activated isomers of nascent CH_3OONO^* formed by the recombination reaction.

mentioned earlier.[34,35] The survival probability curves for the two isomers (Figure 5) show that they behave much like each other, although they differ somewhat during the "damped oscillation" that takes place during the first picosecond. The fact that both isomers show that oscillations and isomerization are not very important suggests that the general results of this study are not affected by the absence of the intrinsic barrier to decomposition of *trans*-CH_3OONO on the model PES.

In Figure 5, the cis isomer clearly shows damped oscillations with a period of ~0.1 ps, which corresponds to a vibrational frequency of ~330 cm^{-1}. This is about equal to the second and third lowest vibrational frequencies in *cis*-CH_3OONO (see Table 2), but considering the strong anharmonicity that accompanies bond-breaking it could be associated with any of the vibrations. Interestingly, the trans isomer shows nonexponential decay but only a hint of oscillation. In addition, the trans isomer reacts a little slower than the cis. Both minor differences could be explained if energy is transferred by IVR from the new bond to the methyl group vibrational modes more rapidly in the trans isomer. The low vibrational frequencies of the two isomers are very similar except for the third lowest frequency, which is 93 cm^{-1} higher in the cis isomer (286 versus 193 cm^{-1}), and the eighth lowest, which is 133 cm^{-1} higher in the cis isomer (778 versus 645 cm^{-1}). It is possible that these differences affect

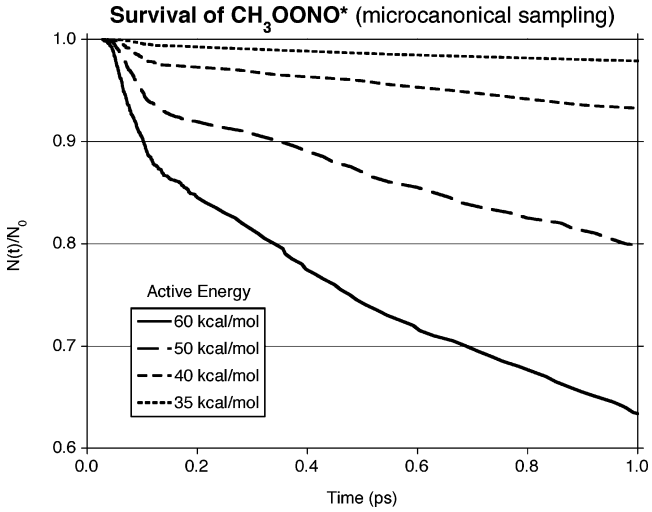

Figure 6. Population decay curves for cis-CH_3OONO^* excited microcanonically at total energy E.

the IVR rate. We speculate that replacing the methyl group with an H atom (i.e., peroxynitrous acid), will result in more prominent oscillations in the reaction rate.

Chemical activation is well known to produce non-RRKM kinetics.[68−77] This is because of the excitation energies, which are often extremely large, and because the nascent distribution of excited species is confined to a very limited region of the available phase space. Often, the reaction rate is faster than predicted by RRKM theory,[38,59] but it has been suggested[78] that an upper limit of $k_{max} \approx 2\omega^* c$ exists to the rate of reaction (where ω^* is a characteristic reciprocal wavelength (wavenumber) related to the reaction coordinate and c is the speed of light), regardless of the excitation energy. With this assumption, the present results for $k_{eff}(E,0)$ are consistent with $\omega^* \approx 300-400$ cm^{-1}, in good agreement with the period of the damped oscillation observable for the cis isomer.

In this hyperdimensional system, it is very difficult to track the energy flow. We attempted to do so by monitoring the mean-square displacement of several individual bonds (C−H, C−O, new N−O, O−O) over time. Our group has previously used this method successfully to monitor the vibrational energy in a bond.[54−56] Unfortunately, the results obtained for CH_3OONO^* are too noisy to allow for interpretation. This is because the excited molecules react so quickly that the number of surviving complexes is too small to provide good averages.

In any event, the dramatic time-dependence of the effective rate constant is quite different from RRKM theory predictions. The damped oscillation is also not predicted by RRKM theory. Both of these phenomena are evidence for non-RRKM dynamics on the model PES.

To test whether the RO−ONO dissociation is an "intrinsic" non-RRKM reaction[59] and to assess the effects of anharmonicity, we calculated batches of trajectories initialized with microcanonical energy distributions in *cis*-CH_3OONO. The resulting population decays showed a fast transient followed by a nearly exponential decay, as shown in Figure 6. The brief delay times in Figure 6 are due to the criterion for dissociation: the O−O bond length ≥2.5 Å, as discussed earlier in the context of capture and dissociation. The initial rate constant $k_{\mu can}(E)$ corresponds to the initial microcanonical energy distribution. The nonexponential decay is due to rapid relaxation of the initial microcanonical energy distribution to a steady-state intramolecular energy distribution with corresponding decay rate constant $k_{ss}(E)$. This is the signature of an intrinsic non-RRKM

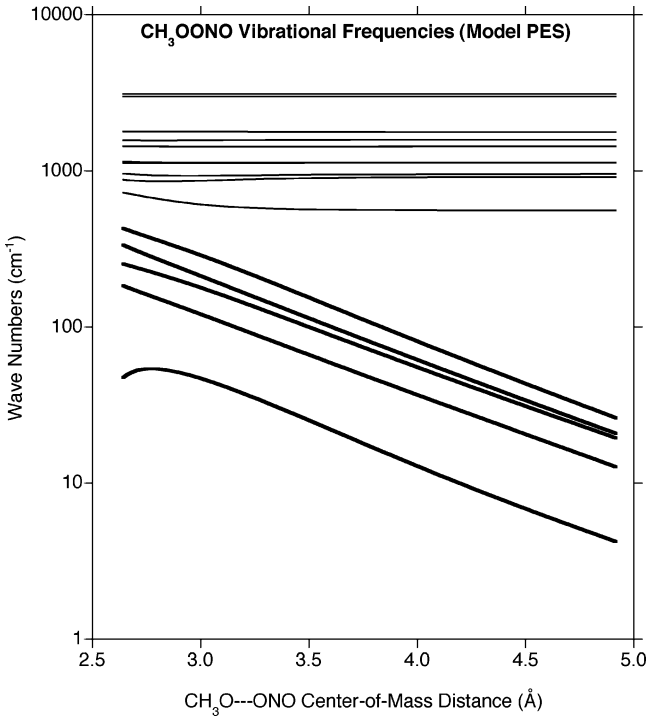

Figure 7. Vibrational frequencies orthogonal to the reaction path on the model PES.

reaction.[59] Rate constant $k_{\mu can}(E)$ was obtained from the slope of a straight line fitted to the initial brief transient and rate constant $k_{ss}(E)$ was obtained by fitting the decay curves to an exponential over the next ~90% of the population decay. These rate constants are shown in Figure 4. At lower energies, the initial nonexponential transient is too brief for accurate determination of $k_{\mu can}(E)$. Inspection of Figure 4 shows that the ratio $k_{\mu can}(E)/k_{ss}(E)$ is ~2.7, indicating that slow IVR significantly reduces the rate constant for dissociation.

The steady-state rate constant following microcanonical excitation, $k_{ss}(E)$, tends to fall below $k_{eff}(E,\infty)$ (steady-state rate constant following chemical activation) by about a factor of ~2−3. This minor discrepancy may occur because the initial chemical activation distribution did not fully relax during the simulations, while the initial microcanonical distribution does not require as much time to relax.

Harmonic μVTST Calculations. These calculations were carried out according to the protocols described above. The first step in the procedure was to use *VENUS96* to find the steepest descent path or minimum energy path (MEP), in mass-weighted Cartesian coordinates. Principal moments of inertia and harmonic vibrational frequencies normal to the MEP were calculated using the modules in *VENUS96*. The vibrational frequencies are shown in Figure 7. In the figure, the "disappearing frequencies", which are associated with the five relative coordinates (not including the O−O bond stretch) between the RO and NO_2, are clearly approaching zero as the center of mass distance increases. The near-exponential dependence at longer range is very similar to the that found in other systems,[41] as first pointed out by Quack and Troe.[79] Although the disappearing frequencies correlate with the rotations of the RO and NO_2,[41] they are treated here as harmonic oscillators for the purpose of calculating the sum of states.

Rate constants, $k_{har}(E)$, obtained using Method I and Method II, differ in the way the K-rotor is treated, as described above. The two methods give results that differ by less than 20%. The results obtained using Method II are presented in Figure 4 for comparison with the QCT results. At the three energies at which $k_{\mu can}(E)$ could be determined, $k_{har}(E)$ is approximately 1 order of magnitude larger. This difference is due to vibrational anharmonicity and to the neglect of the conversion of the "disappearing vibrations" into rotations, as described above. Vibrational anharmonicity is expected to increase in both the density of states of the reactant and the sum of states of the transition state, but the latter effect dominates because of the higher active energy in the excited reactant. If hindered rotors had been used to calculate the sum of states, then $k_{har}(E)$ would likely have been a little larger, increasing the difference between $k_{har}(E)$ and $k_{\mu can}(E)$. Therefore, we conclude that anharmonicity is probably responsible for the approximately order-of-magnitude difference.

At high energies, the picture is quite different. At high energy, the $<k_{eff}(E)>$ from QCT calculations is ~2.3 ps^{-1} at $E = 59$ kcal mol^{-1}. In contrast, the $k(E)$ from μVTST is ~14 ps^{-1} at the same energy. This value is more than twice as large as the fast initial $k_{eff}(E,0)$ at that energy and six times as great as $<k_{eff}(E)>$. Thus RRKM theory overestimates the dissociation rate constant at energies corresponding to the zero-point energy of the reactants, and the discrepancy grows as the energy is further increased. This adds to the other dynamical evidence of non-RRKM behavior.

Conclusions

The central conclusion from this study is that the population of highly excited CH_3OONO^* complexes formed by chemical activation decay rapidly by non-RRKM kinetics. Two characteristics of the decay support the conclusion that RRKM theory is inaccurate for this system. First, the rate constant for reaction is initially very large, but decreases by orders of magnitude as time progresses, while RRKM theory predicts a time-independent rate constant. Second, during the first picosecond the population decay behaves like a damped oscillation, instead of the exponential decay predicted by RRKM theory.

Chemical activation systems are well known for producing non-RRKM kinetics. This comes about because the nascent population of excited molecules has a large amount of energy. We surmise that damped oscillations are observable in the present work because the nascent molecules are formed in a narrow energy distribution and in a restricted range of initial geometries. We speculate that the oscillations will be more prominent if the methyl group is replaced by a single atom, as in peroxynitric acid (HOONO).

A second important conclusion from this study is that vibrational anharmonicity associated with the highly excited ROONO* complex is very important in increasing the density of states and hence reducing the rate constant well below $k_{har}(E)$. These results provide a physical rationale for using slower rate constants for decomposition of ROONO in master equation simulations. Zhang et al.[35] used extremely slow rate constants for ROONO decomposition to better fit the experimental data, but they could not provide a physical justification. Barker et al.[34] used more conventional decomposition rate constants (including some anharmonicity) but were able to fit the experimental data only by using unphysically small energy transfer parameters. Increasing the lifetime of ROONO* will tend to make collisional deactivation of ROONO* more important than in the simulations reported by Barker et al. This will enable the use of more reasonable energy transfer parameters and will make the simulations more similar to those of Zhang et al.

Whether the effects found in the present work are large enough to fully explain the anomalies in the master equation

simulations can only be ascertained by carrying out new simulations. The analytical PES used in the present work is plausible and fits the geometries and vibrational frequencies for the equilibrium structures very accurately, but parametrization of the anharmonic interactions at high energy and accurate values for the individual attenuation constants are needed. Improvements along these lines are planned.

Note Added in Proof: In a recent paper, Arenas et al. [Arenas, J. F.; Avila, F. J.; Otero, J. C.; Pelaez, D.; Soto, J. *J. Phys. Chem. A* **2008**, *112*, 249−255] located a conical intersection near the geometry of the intrinsic energy barrier found by several groups for the *trans*-RO-ONO bond fission. Arenas et al. conclude that the energy barrier is an artifact that is due to the use of single configuration wavefunctions when a conical intersection is present. Thus the topology of the model PES used in the present work may be reasonably accurate.

Acknowledgment. We thank the National Science Foundation (Atmospheric Chemistry Division) for funding (Award Number ATM 0344102). We also thank Neil Donahue for commenting on the manuscript and Bill Hase for several helpful suggestions.

References and Notes

(1) Darnall, K. R.; Carter, W. P. L.; Winer, A. M.; Lloyd, A. C.; J. N. Pitts, J. *J. Phys. Chem.* **1976**, *80*, 1948−1950.

(2) Chen, X.; Hulbert, D.; Shepson, P. B. *J. Geophys. Res., [Atmos.]* **1998**, *103*, 25563−25568.

(3) Grossenbacher, J. W.; Barket, D. J.; Shepson, P. B.; Carroll, M. A.; Olszyna, K.; Apel, E. *J. Geophys. Res., [Atmos.]* **2004**, *109*.

(4) Fuentes, J. D.; Wang, D.; Bowling, D. R.; Potosnak, M.; Monson, R. K.; Goliff, W. S.; Stockwell, W. R. *J. Atmos. Chem.* **2007**, *56*, 165−185.

(5) Horowitz, L. W.; Fiore, A. M.; Milly, G. P.; Cohen, R. C.; Perring, A.; Wooldridge, P. J.; Hess, P. G.; Emmons, L. K.; Lamarque, J. F. *J. Geophys. Res., [Atmos.]* **2007**, *112*.

(6) Lim, Y. B.; Ziemann, P. J. *Environ. Sci. Technol.* **2005**, *39*, 9229−9236.

(7) Kroll, J. H.; Chan, A. W. H.; Ng, N. L.; Flagan, R. C.; Seinfeld, J. H. *Environ. Sci. Technol.* **2007**, *41*, 3545−3550.

(8) Lee, A.; Goldstein, A. H.; Kroll, J. H.; Ng, N. L.; Varutbangkul, V.; Flagan, R. C.; Seinfeld, J. H. *J. Geophys. Res., [Atmos.]* **2006**, *111*.

(9) Olcese, L. E.; Penner, J. E.; Sillman, S. *Atmos. Chem. Phys.*, submitted for publication, 2007.

(10) Atkinson, R.; Cox, R. A.; Crowley, J.; Hampson, R. F.; Hynes, R. G.; Jenkin, M. E.; Kerr, J. A.; Rossi, M. J.; Troe, J. *Summary of Evaluated Kinetic and Photochemical Data for Atmospheric Chemistry. Section II - Organic Reactions*; IUPAC Subcommittee for Gas Kinetic Data Evaluation for Atmospheric Chemistry: Cambridge, U.K., 2006. *http://www.iupac-kinetic.ch.cam.ac.uk/index.html*.

(11) Aschmann, S. M.; Long, W. D.; Atkinson, R. *J. Phys. Chem. A* **2006**, *110*, 6617−6622.

(12) Atkinson, R.; Arey, J. *Chem. Rev.* **2003**, *103*, 4605−4638.

(13) Atkinson, R.; Baulch, D. L.; Cox, R. A.; Crowley, J. N.; Hampson, R. F.; Hynes, R. G.; Jenkin, M. E.; Rossi, M. J.; Troe, J. *Atmos. Chem. Phys.* **2006**, *6*, 3625−4055.

(14) Sander, S. P.; Friedl, R. R.; Ravishankara, A. R.; Golden, D. M.; Kolb, C. E.; Kurylo, M. J.; Molina, M. J.; Moortgat, G. K.; Finlayson-Pitts, J. B.; Wine, P. H.; Huie, R. E.; Orkin, V. L. *Chemical Kinetics and Photochemical Data for Use in Stratospheric Modeling*, Evaluation Number 15; Jet Propulsion Laboratory: Pasadena, CA, 2006, *http://jpldataeval.jpl.nasa.gov/*.

(15) Tyndall, G. S.; Cox, R. A.; Granier, C.; Lesclaux, R.; Moortgat, G. K.; Pilling, M. J.; Ravishankara, A. R.; Wallington, T. J. *J. Geophys. Res., [Atmos.]* **2001**, *106*, 12157−12182.

(16) Nizkorodov, S. A.; Wennberg, P. O. *J. Phys. Chem. A* **2002**, *106*, 855−859.

(17) Bean, B. D.; Mollner, A. K.; Nizkorodov, S.; Nair, G.; Okumura, M.; Sander, S. P.; Peterson, K. A.; Francisco, J. S. *J. Phys. Chem. A* **2003**, *107*, 6974−6985.

(18) Pollack, I. B.; Konen, I. M.; Li, E. X. J.; Lester, M. I. *J. Chem. Phys.* **2003**, *119*, 9981−9984.

(19) Fry, J. L.; Nizkorodov, S. A.; Okumura, M.; Roehl, C. M.; Francisco, J. S.; Wennberg, P. O. *J. Chem. Phys.* **2004**, *121*, 1432−1448.

(20) Mathews, J.; Sinha, A.; Francisco, J. S. *J. Chem. Phys.* **2004**, *120*, 10543−10553.

(21) Matthews, J.; Sinha, A. *J. Chem. Phys.* **2005**, *122*, 104313.

(22) Konen, I. M.; Pollack, L. B.; Li, E. X. J.; Lester, M. I.; Varner, M. E.; Stanton, J. F. *J. Chem. Phys.* **2005**, *122*, 094320/094321−094320/094316.

(23) Konen, I. M.; Li, E. X. J.; Stephenson, T. A.; Lester, M. I. *J. Chem. Phys.* **2005**, *123*, 204318/204311−204318/204311.

(24) Zhang, X.; Nimlos, M. R.; Ellison, G. B.; Varner, M. E.; Stanton, J. F. *J. Chem. Phys.* **2006**, *124*, 084305/084301−084305/084307.

(25) Zhao, Y.; Houk, K. N.; Olsen, L. P. *J. Phys. Chem. A* **2004**, *108*, 5864−5871.

(26) Ellison, G. B.; Herbert, J. M.; McCoy, A. B.; Szalay, P. G.; Stanton, J. F. *J. Phys. Chem. A* **2004**, *108*, 7639−7642.

(27) McGrath, M. P.; Rowland, F. S. *J. Chem. Phys.* **2005**, *122*, 134312/134311−134312/134314.

(28) McCoy, A. B.; Fry, J. L.; Francisco, J. S.; Mollner, A. K.; Okumura, M. *J. Chem. Phys.* **2005**, *122*, 104311/104311−104311/104314.

(29) Smith, G. P.; Golden, D. M. *Int. J. Chem. Kinet.* **1978**, *10*, 489.

(30) Golden, D. M.; Smith, G. P. *J. Phys. Chem. A* **2000**, *104*, 3991−3997.

(31) Golden, D. M.; Barker, J. R.; Lohr, L. L. *J. Phys. Chem. A* **2003**, *107*, 11057−11071.

(32) Zhang, J.; Donahue, N. M. *J. Phys. Chem. A* **2006**, *110*, 6898−6911.

(33) Lohr, L. L.; Barker, J. R.; Shroll, R. M. *J. Phys. Chem. A.* **2003**, *107*, 7429−7433.

(34) Barker, J. R.; Lohr, L. L.; Shroll, R. M.; Reading, S. *J. Phys. Chem. A.* **2003**, *107*, 7434−7444.

(35) Zhang, J. Y.; Dransfield, T.; Donahue, N. M. *J. Phys. Chem. A* **2004**, *108*, 9082−9095.

(36) Barker, J. R.; Golden, D. M. *Chem. Rev.* **2003**, *103*, 4577−4591.

(37) Chen, C.; Shepler, B. C.; Braams, B. J.; Bowman, J. M. *J. Chem. Phys.* **2007**, *127*, 104310.

(38) Baer, T.; Hase, W. L. *Unimolecular Reaction Dynamics. Theory and Experiments*; Oxford University Press: New York, 1996.

(39) Forst, W. *Theory of Unimolecular Reactions*; Academic Press: New York, 1973.

(40) Forst, W. *Unimolecular Reactions. A Concise Introduction*; Cambridge University Press: Cambridge, 2003.

(41) Holbrook, K. A.; Pilling, M. J.; Robertson, S. H. *Unimolecular Reactions*, 2nd ed.; Wiley: Chichester, England, 1996.

(42) Robinson, P. J.; Holbrook, K. A. *Unimolecular Reactions*; Wiley-Interscience: New York, 1972.

(43) Gilbert, R. G.; Smith, S. C. *Theory of Unimolecular and Recombination Reactions*; Blackwell Scientific: Oxford, 1990.

(44) Atkinson, R.; Aschmann, S. M.; Carter, P. L.; Pitts, J. N., Jr. *J. Phys. Chem.* **1982**, *86*, 4563−4569.

(45) Atkinson, R.; Carter, W. P. L.; Winer, A. M. *J. Phys. Chem.* **1983**, *87*, 2012−2018.

(46) Atkinson, R.; Aschmann, S. M.; Carter, W. P. L.; Winer, A. M.; Pitts, J. N., J. *Int. J. Chem. Kinet.* **1984**, *16*, 1085−1101.

(47) Atkinson, R.; Aschmann, S. M.; Winer, A. M. *J. Atmos. Chem.* **1987**, *5*, 91−102.

(48) Golden, D. M.; Barker, J. R.; Lohr, L. L. *J. Phys. Chem. A* **2004**, *108*, 8552.

(49) Dixon, D. A.; Feller, D.; Zhan, C.-G.; Francisco, J. S. *J. Phys. Chem. A* **2002**, *106*, 3191−3196.

(50) Lesar, A.; Hodoek, M.; Drougas, E.; Kosmas, A. M. *J. Phys. Chem. A* **2006**, *110*, 7898 -7903.

(51) Lesar, A.; Salta, Z.; Kovačič, S.; Kosmas, A. M. *Chem. Phys. Lett.* **2007**, *441*, 268−275.

(52) Hase, W. L.; Mrowka, G.; Brudzynski, R. J.; Sloane, C. S. *J. Chem. Phys.* **1978**, *69*, 3548−3562.

(53) Hase, W. L.; Duchovic, R. J.; Hu, X.; Komornicki, A.; Lim, K. F.; Lu, D.-H.; Peslherbe, G. H.; Swamy, K. N.; Linde, S. R. V.; Varandas, A.; Wang, H.; Wolf, R. J. *Quantum Chem. Program Exch. Bull.* **1996**, *16*.

(54) Liu, Y.; Lohr, L. L.; Barker, J. R. *J. Phys. Chem. B* **2005**, *109*, 8304−8309.

(55) Liu, Y.; Lohr, L. L.; Barker, J. R. *J. Phys. Chem. A* **2006**, *110*, 1267−1277.

(56) Stimac, P. J.; Barker, J. R. *J. Phys. Chem. A* **2006**, *110*, 6851−6859.

(57) Straatsma, T. P. A., E.; Windus, T. L.; Bylaska, E. J.; de Jong, W.; Hirata, S.; Valiev, M.; Hackler, M. T.; Pollack, L.; Harrison, R. J.; Dupuis, M.; Smith, D. M. A.; Nieplocha, J.; Tipparaju, V.; Krishnan, M.; Auer, A. A.; Brown, E.; Cisneros, G.; Fann, G. I.; Fruchtl, H.; Garza, J.; Hiaro, K.; Kendall, R.; Nichols, J. A.; Tsemekhman, K.; Wolinski, K.; Anchell, J.; Bernholdt, D.; Borowski, P.; Clark, T.; Clerc, D.; Dachsel, H.; Deegan, M.; Dyall, K.; Elwood, D.; Glendening, E.; Gutowski, M.; Hess, A.; Jaffe, J.; Johnson, B.; Ju, J.; Kobayashi, R.; Kutteh, R.; Lin, Z.; Littlefield, R.; Long, X.; Meng, B.; Nakajima, T.; Niu, S. R., M.; Sandrone, G.; Stave, M.; Taylor, H.; Thomas, G.; van Lenthe, J.; Wong, A.; Zhang, Z. *NWChem*,

A Computational Chemistry Package for Parallel Computers, Version 4.6; Pacific Northwest National Laboratory: Richland, Washington, 2004.
(58) Hase, W. L.; Buckowski, D. G. *Chem. Phys. Lett.* **1980**, *74*, 284−287.
(59) Bunker, D. L.; Hase, W. L. *J. Chem. Phys.* **1973**, *59*, 4621−4632.
(60) Liu, J.; Barker, J. R. *J. Phys. Chem. A* **2007**, *111*, 8689−8698.
(61) Peslherbe, G. H.; Hase, W. L. *J. Chem. Phys.* **1996**, *105*, 7432−7447.
(62) Hu, X.; Hase, W. L. *J. Chem. Phys.* **1991**, *95*, 8073−8082.
(63) Wang, H. B.; Zhu, L.; Hase, W. L. *J. Phys. Chem.* **1994**, *98*, 1608−1619.
(64) Wang, H. B.; Hase, W. L. *J. Am. Chem. Soc.* **1997**, *119*, 3093−3102.
(65) Zhu, L.; Hase, W. L. *Chem. Phys. Lett.* **1990**, *175*, 117−124.
(66) Miller, W. H. *J. Am. Chem. Soc* **1979**, *101*, 6810−6814.
(67) Aubanel, E. E.; Wardlaw, D. M.; Zhu, L.; Hase, W. L. *Int. Rev. Phys. Chem.* **1991**, *10*, 249−286.
(68) Rabinovitch, B. S.; Meagher, J. F.; Chao, K.-J.; Barker, J. R. *J. Chem. Phys.* **1974**, *60*, 2932−2933.
(69) Oref, I.; Rabinovitch, B. S. *Acc. Chem. Res.* **1979**, *12*, 166−175.
(70) Rynbrandt, J. D.; Rabinovitch, B. S. *J. Phys. Chem.* **1970**, *74*, 4175−4176.
(71) Rynbrandt, J. D.; Rabinovitch, B. S. *J. Phys. Chem.* **1971**, *75*, 2164−2171.
(72) Carpenter, B. K. *Ann. Rev. Phys. Chem.* **2005**, *56*, 57−89.
(73) Carpenter, B. K. *J. Phys. Org. Chem.* **2003**, *16*, 858−868.
(74) Carpenter, B. K. *Angew. Chem., Int. Ed.* **1998**, *37*, 3340−3350.
(75) Peslherbe, G. H.; Wang, H.; Hase, W. L. *J. Chem. Phys.* **1995**, *102*, 5626−5635.
(76) Wester, R.; Bragg, A. E.; Davis, A. V.; Neumark, D. M. *J. Chem. Phys.* **2003**, *119*, 10032−10039.
(77) Vayner, G.; Addepalli, S. V.; Song, K.; Hase, W. L. *J. Chem. Phys.* **2006**, *125*, 014317.
(78) Barker, J. R.; Stimac, P. J.; King, K. D.; Leitner, D. M. *J. Phys. Chem. A* **2006**, *110*, 2944−2954.
(79) Quack, M.; Troe, J. *Ber. Bunsen-Ges. Phys. Chem.* **1977**, *81*, 329−337.
(80) Benson, S. W. *J. Chem. Educ.* **1965**, *42*, 502−518.
(81) Preiskorn, A.; Thompson, D. L. *J. Chem. Phys.* **1989**, *91*, 2299−2307.
(82) McKee, M. L. *J. Am. Chem. Soc.* **1986**, *108*, 5784−5792.
(83) Cornell, W. D.; Cieplak, P.; Bayly, C. I.; Gould, I. R.; Merz, K. M.; Ferguson, D. M.; Spellmeyer, D. C.; Fox, H.; Caldwell, J. W.; Kollman, P. A. *J. Am. Chem. Soc.* **1995**, *117*, 5179−5197.